

# mitoTALEN reduces the mutant mtDNA load in neurons

Sandra R. Bacman,<sup>1</sup> Jose Domingo Barrera-Paez,<sup>2</sup> Milena Pinto,<sup>1</sup> Derek Van Booven,<sup>3</sup> James B. Stewart,<sup>4</sup> Anthony J. Griswold,<sup>3</sup> and Carlos T. Moraes<sup>1,5</sup>

<sup>1</sup>Department of Neurology, University of Miami Miller School of Medicine, Miami, FL, USA; <sup>2</sup>Graduate Program in Human Genetics and Genomics, University of Miami Miller School of Medicine, Miami, FL, USA; <sup>3</sup>John P. Hussman Institute for Human Genomics, University of Miami Miller School of Medicine, Miami, FL, USA; <sup>4</sup>Biosciences Institute, Faculty of Medical Sciences, Wellcome Centre for Mitochondrial Research, Newcastle University, Newcastle upon Tyne, UK; <sup>5</sup>Department of Cell Biology, University of Miami Miller School of Medicine, Miami, FL, USA

**Mutations within mtDNA frequently give rise to severe encephalopathies. Given that a majority of these mtDNA defects exist in a heteroplasmic state, we harnessed the precision of mitochondrial-targeted TALEN (mitoTALEN) to selectively eliminate mutant mtDNA within the CNS of a murine model harboring a heteroplasmic mutation in the mitochondrial tRNA alanine gene (m.5024C>T). This targeted approach was accomplished by the use of AAV-PHP.eB and a neuron-specific synapsin promoter for effective neuronal delivery and expression of mitoTALEN. We found that most CNS regions were effectively transduced and showed a significant reduction in mutant mtDNA. This reduction was accompanied by an increase in mitochondrial tRNA alanine levels, which are drastically reduced by the m.5024C>T mutation. These results showed that mitochondrial-targeted gene editing can be effective in reducing CNS-mutant mtDNA *in vivo*, paving the way for clinical trials in patients with mitochondrial encephalopathies.**

## INTRODUCTION

Mitochondria are double-membrane organelles involved in essential cellular functions. They produce most cellular ATP through the oxidative phosphorylation (OXPHOS) system. In addition, the mitochondrial network regulates intercellular communication and controls different metabolic pathways such as calcium buffering and apoptosis, cellular health, and genomic integrity. Mitochondria carry their own genome, which consists of multiple copies of a double-stranded circular DNA molecule (mtDNA).<sup>1,2</sup> Mammalian mtDNA encodes only 37 genes, including 2 ribosomal RNAs, 22 transfer RNAs, and 13 mitochondrial OXPHOS complex proteins, while the rest of the mitochondrial proteome, which includes approximately 1,500 proteins, is encoded by the nuclear DNA.<sup>3,4</sup> Mitochondrial diseases can be genetically classified in two major categories, depending on whether the mutations occur in the mitochondrial or the nuclear genome.<sup>5</sup> The prevalence of mitochondrial diseases is estimated to be 1 in 5,000,<sup>6</sup> and mtDNA mutations are responsible for at least one-half of them.<sup>7</sup> Pathogenic mtDNA variants are maternally inherited and often co-exist with wild-type mtDNA molecules, a state known as heteroplasmy.<sup>8,9</sup>

Even in a single patient, different cells, tissues, and organs can have varying levels of mtDNA heteroplasmy.<sup>6</sup> Clinical and biochemical manifestations occur when the ratio of mutant to wild-type mtDNA exceeds approximately 4:1.<sup>5</sup> Heteroplasmic mtDNA mutations in genes encoding for OXPHOS subunits, tRNAs, and rRNAs have been linked to various clinical manifestations.<sup>10</sup>

Several gene manipulation strategies have been developed by our group and others to selectively reduce the levels of mutant mtDNA while allowing the levels of wild-type mtDNA to increase, including mitochondrial-targeted nucleases (mitoNucleases) and mitochondrial-targeted base editors (mitoBase Editors). MitoNucleases induce a double-strand break (DSB) in the mutant mtDNA while mitoBase Editors promote base transitions without creating DSBs.<sup>11</sup>

Several types of mitoNucleases have been reported, including: mitochondrial-targeted restriction endonucleases, mitochondrial-targeted TALEN (mitoTALEN), zinc finger nucleases (mitoZFNs) and meganucleases, all of which have been shown to eliminate mutant mtDNA *ex vivo* and *in vivo* (reviewed in<sup>9,12,13</sup>).

MitoTALENs have shown promising results in cultured cells and *in vivo*.<sup>12</sup> It was used to eliminate mutant mtDNA in the muscle of a heteroplasmy mouse model carrying the m.5024C>T mutation in the tRNA<sup>Ala</sup> gene. Delivery of AAV9-mitoTALEN either intramuscularly or intravenously resulted in the reduction of the mutant mtDNA load both in heart and skeletal muscle.<sup>14</sup>

Because many mitochondrial disorders affect the CNS,<sup>15,16</sup> in the present study we aimed to eliminate the mutant mtDNA in the brain. No mouse model exhibiting a mtDNA heteroplasmic mutation that induces a clinical phenotype in the brain is currently available. Therefore, we used an existing mouse model that carries a heteroplasmic

Received 5 April 2023; accepted 29 January 2024;  
<https://doi.org/10.1016/j.omtn.2024.102132>.

**Correspondence:** Carlos T. Moraes, Department of Neurology, University of Miami Miller School of Medicine, Miami, FL, USA.

**E-mail:** [CMoraes@med.miami.edu](mailto:CMoraes@med.miami.edu)



tRNA<sup>Ala</sup> mutation (m.5024C>T). This base change disrupts the same base pair in the acceptor stem of tRNA<sup>Ala</sup> as the pathogenic m.5650G>A mutation found in human patients with a mitochondrial disease.<sup>17,18</sup> Moreover, despite not having overt clinical features, this model has a well established molecular phenotype, which is a decrease in mitochondrial tRNA<sup>Ala</sup> levels.<sup>14</sup>

## RESULTS

### Promoter selection for high expression in neurons

To evaluate which promoter was more effective for robust neuronal expression, three different promoters were tested: neuronal-specific SYN (human synapsin), and ubiquitous promoters CBh (a modified form of the chicken beta actin promoter), and cytomegalovirus (CMV) (Figure 1A). For gene delivery, we used AAV.PHP.eB, which was reported to efficiently deliver genes to the CNS of C57BL/6 mice.<sup>19–21</sup> Three recombinant PHP.eB-eGFP ( $2–3 \times 10^{13}$  vg/kg), containing an eGFP gene driven by either of the three different promoters were injected retro-orbitally (which rapidly drains into the venous system) in P16–18 mice. Mice were sacrificed 6 weeks after injection (P58–60) and expression in different tissues was evaluated. The SYN promoter drove high expression of eGFP in brain; relatively lower expression in heart, kidney, and skeletal muscle; and no detectable expression in liver (Figures 1B and 1C). CBh promoter also drove robust expression in the CNS (Figures 1B and 1C), but also strong expression in the liver. The CMV promoted poor expression in the CNS (Figures 1B and 1C).

We then analyzed the eGFP expression driven by the SYN promoter in several brain regions and we detected stronger expression in cortex, hippocampus and striatum/midbrain (Figure 1D). This relatively high level of delivery and expression could also be observed by the intense brain fluorescence of P60 mice injected with AAV-PHP.eB-SYNpr-eGFP at P16–18 (Figure 1E). Although the CBh promoter also drove robust expression in the CNS, we decided to use the SYN promoter, as it did not drive expression in the liver, and also to better assess changes in the neuronal population.

### mitoTALEN monomers localized to mitochondria

We assembled two recombinant AAV plasmids encoding for mitoTALENs by a combination of gene synthesis and INFUSION ligations (see Materials and methods). The TAL DNA-binding sequences were similar to the ones previously used to successfully eliminate the mutant m.5024T mtDNA in muscle of heteroplasmic mice.<sup>14</sup> In the present study, monomer 134 was lengthened to contain 11.5 RVDs (Figure 2A), with the final construct still within the limits of AAV packaging. The MitoTALEN architecture requires two monomers. Monomer 134 carried a FLAG tag and a Fok I CCK version of the heterodimeric endonuclease, while monomer 132 carried an HA tag, a Fok I NEL version of the endonuclease, and eGFP downstream of a T2A sequence (Figure 2B). Both constructs expression was driven by the human SYN promoter and directed to mitochondria by a Cox8/Sub9 (C8S9) mitochondrial targeting sequence (MTS) (Figure 2B). COS7 cells were transiently transfected with each individual plasmid. Even though the SYN promoter is not strongly expressed in

cultured COS7 cells, the high levels of plasmid after transient transfections produced enough expression to show that they co-localizing with mitotracker, a cationic dye that accumulates in mitochondria (Figure 2C). The recombinant transgenes, with their predicted molecular weights, could also be observed in western blots (Figure 2D).

### AAV-PHP.eBPHP.eB-SYN-mitoTALEN is expressed in the brain of mice injected through the venous system

We next produced AAV-PHP.eB viruses for each of the monomers and injected them (combined) into P16-P18 mice, as described above. Because one of the monomers also expresses eGFP, we could observe eGFP staining in the cortex of mice systemically injected with both AAV-PHP.eB-SYNpr-mitoTALEN monomers after 6 weeks (Figure S1A). As expected, stained cells had a neuronal morphology. Double staining with the neuronal marker NeuN confirmed these findings (Figure S1B). Specific expression of Flag, HA, and GFP were also observed in cortex, hippocampus, and striatum/midbrain, with lower expression in cerebellum and spinal cord (Figures 3A and S2A). No expression was observed in the other tissues analyzed, including heart, kidney, tibialis anterior (TA) muscle and liver (Figures 3A and S2A). A band migrating slightly higher than expected was observed in heart samples (observed in both mitoTALEN and eGFP [which has no FLAG]) (Figure S2A). It seems to be an artifact as it was not observed in other similar blots (e.g., Figure 3A). Similar results were observed at 24 weeks after injection (Figure S2B). Western blots for the neuronal marker TUJ1 (Figure 3A), showed the neuronal marker in the same tissues mitoTALEN was expressed.

Using digital PCR (dPCR), we quantified AAV DNA levels and found relatively high levels in CNS tissues, particularly in the cortex and striatum and midbrain. Figure 3B shows the ratios of the AAV DNA specific for each AAV-PHP.eB-SYNpr-mitoTALEN monomer at 6 weeks after injection (Flag and HA) normalized to the transthyretin (TTR) nuclear gene. AAV DNA levels roughly matched the relative distribution of protein expression shown in Figure 3A, but a perfect match among different CNS regions was not expected given the SYN promoter specificity.

### AAV-PHP.eB-SYNpr-mitoTALEN administration decreased mutant mtDNA levels in brain tissues of heteroplasmic tRNA<sup>Ala</sup> in mice with no changes in the mtDNA copy number

Heteroplasmic mice were systemically injected in the venous system (retro-orbitally) at P16–18 with AAV-PHP.eB-SYNpr-mitoTALEN or AAV-PHP.eB-SYNpr-eGFP and sacrificed at 6, 12, and 24 weeks after injection. DNA was extracted from various CNS and non-CNS tissues and mtDNA heteroplasmy was evaluated by restriction fragment-length polymorphism (RFLP) (Figure S3, raw data in Table S1) and dPCR (Figures 4A and S4, raw data in Table S2). RFLP analysis showed a moderate (approximately 15%–20%), but persistent and significant, decrease in the mutant mtDNA load in all CNS tissues of the AAV-PHP.eB-SYNpr-mitoTALEN-injected mice (Figure S3). This decrease in heteroplasmy was significant in the cortex and hippocampus at 6, 12, and 24 weeks after injection. All these measurements were normalized to the mtDNA

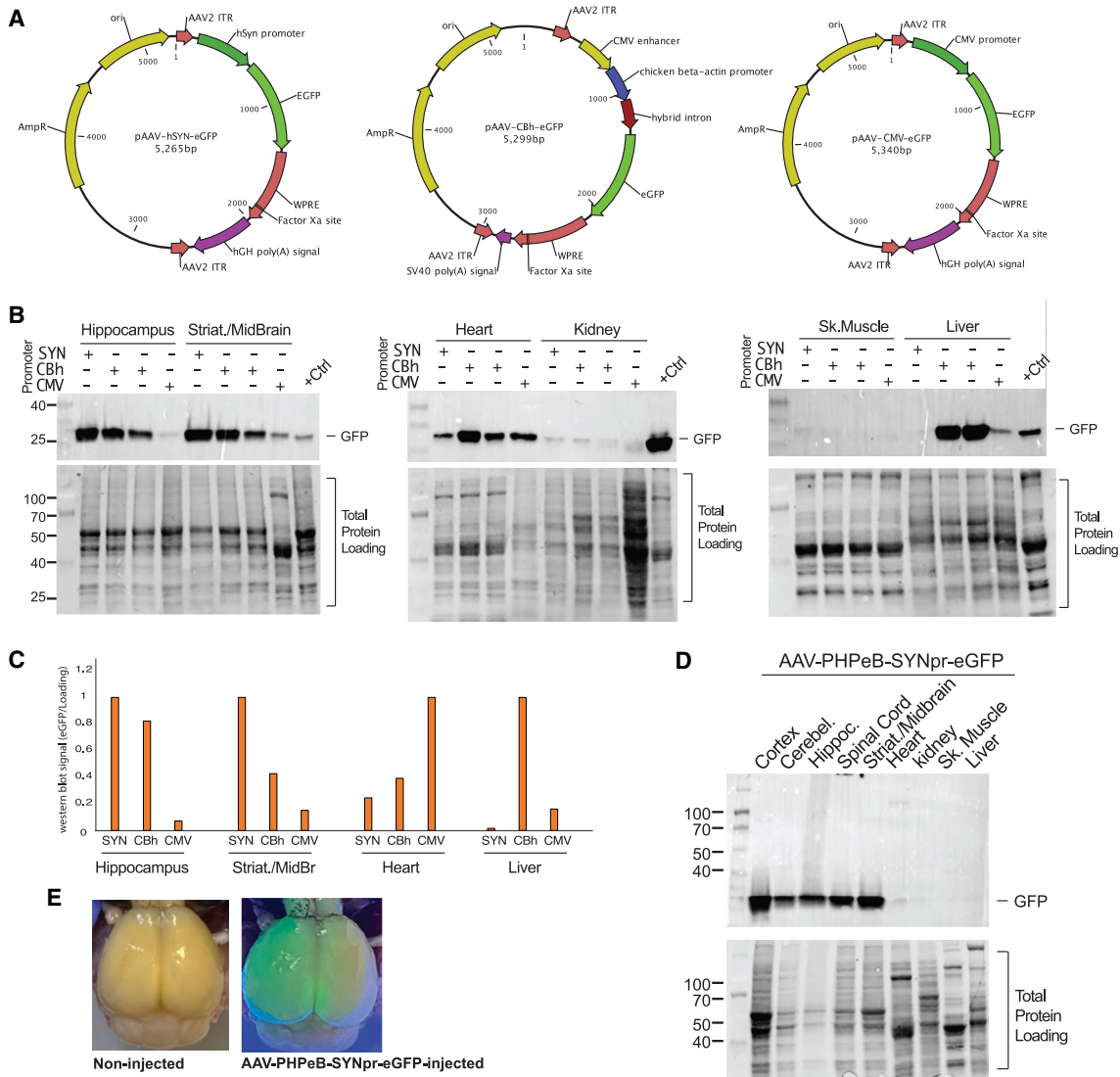


**Figure 1. Evaluating different promoters to target neurons**

(A) Maps of the three recombinant plasmids used to produce AAV-PHP.eB-eGFP expression driven by different promoters: the human neuron-specific synapsin, (SYN), chicken beta actin hybrid (CBh) and CMV promoters. (B) Representative blots probing for eGFP in different tissues. Heteroplasmic mice were injected retro-orbitally at P16–18 and sacrificed 6 weeks later. Different tissues were analyzed for eGFP expression. (C) Quantification of the ratios eGFP/loading normalized to the highest ratio (=1). Tissues with negligible expression of eGFP were not included in the quantitation analysis. (D) Western blot analyzes of eGFP expression in different brain regions of a mouse injected with AAV-PHP.eB-SYNpr-eGFP at 6 weeks post-injection. (E) Brain exposed to UV light showing eGFP expression throughout the cortex 6 weeks after systemic AAV-PHP.eB-SYNpr-eGFP-injected mouse.

heteroplasmy in TA muscle and kidney, tissues that showed no mito-TALEN expression. Similar results were obtained when using dPCR to determine the mutant load (Figure 4A). A significant decrease in the mutant load was observed when comparing Cortex normalized to skeletal muscle (TA) of heteroplasmic mice injected with AAV-PHP.eB-SYNpr-mitoTALEN to the ones injected with AAV-PHP.eB-SYNpr-eGFP. The total mtDNA copy number was simultaneously analyzed in the cortex and no depletion was observed (Figure 4B) at any time point. Examples of the one-dimensional plots

from the dPCR multiplex data to evaluate mtDNA heteroplasmy and copy number are shown in Figure S4.

We ruled out that mtDNA heteroplasmy analysis was affected by nuclear mitochondrial pseudogenes (NUMTS-pseudogenes). As shown in Figure S5, chromosomes 2 and 5 nuclear pseudogene-specific SNVs (corresponding with the m.5040G and m.5029C) were not observed in our mtDNA amplifications from brain DNA, ensuring that the heteroplasmy results originated from the mtDNA.

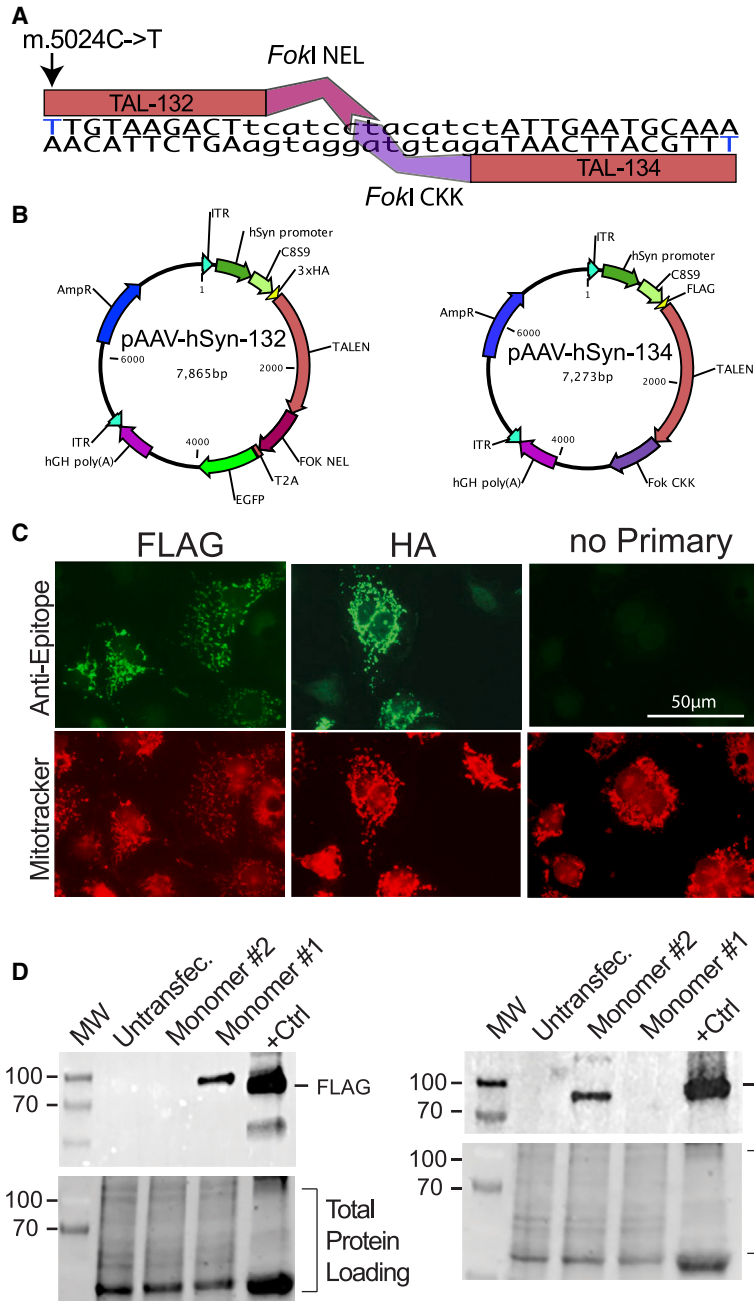


**Figure 2. mitoTALENs specifically target the mitochondria**

(A) Diagram of the TALEN binding region. One monomer (132) has 9.5 RVDs and binds to the mutation sequence (m.5024C>T) (capital/bold); the other monomer (134) has 11.5 RVDs and binds to the WT sequence (capital/bold). The TAL-required "T" ("A" in the reverse strand) at the 5' end is marked in blue. The obligatory heteromeric *FokI* cleaves the DNA in the spacer region. (B) Maps of AAV-PHP.eB plasmids with human synapsin (SYN) promoter used. Both monomers carry a C8S9 MTS but different immune TAGs (FLAG or HA). Monomer #132 has an eGFP gene after a T2A sequence. (C) COS7 cells were immunostained for FLAG or HA 48 h after transfection with each of the plasmids. Cells were co-labelled with mitotracker red before fixation to detect the mitochondrial localization of each monomer. (D) COS7 cells were transfected with each of the two plasmids (individually) and protein expression (FLAG and HA) was detected by western blot 48h after transfection. Predicted size of the monomers were: #134 = 100.9 kDa and #132 = 90.0 kDa.

of heteroplasmic mice and showed that the  $tRNA^{Ala}/tRNA^{Asn}$  ratios in cortex (brain) and TA (skeletal muscle) are strictly and inversely proportional to the levels of the m.5024C>T mutation ( $R > 0.96$ ) (Figure 5A). Next, RNA samples from the cortex and TA muscle from mice sacrificed at 6, 12, and 24 weeks after injection of AAV-PHP.eB-SYNpr-mitoTALEN or AAV-PHP.eB-SYNpr-eGFP were obtained and  $tRNA^{Ala}$  levels were quantified by dPCR of reverse transcribed samples, as outlined above.

Heteroplasmic mice injected with AAV-PHP.eB-SYNpr-mitoTALEN showed an increase (approximately 20%) of  $tRNA^{Ala}/tRNA^{Asn}$  relative levels in brain regions at 6, 12, and 24 weeks after injection (Figure 5B). This CNS/muscle/ $tRNA^{Asn}$  ratio differential was neither observed in heteroplasmic mice injected with AAV-PHP.eB-SYNpr-eGFP nor in wild-type (WT) mice (Figure 5B). This change in  $tRNA^{Ala}$  levels

followed the slope prediction obtained by the calibration depicted in Figure 5A.

#### Screening for nuclear off-target DSBs

As shown in Figure 2, mitoTALEN could be detected only in mitochondria. However, we cannot rule out that a few molecules mis-localize to the nucleus and promote DSBs. Although off-target DSB are more easily detected in cultured cells, using GUIDE-seq<sup>22</sup> or related techniques, we looked for the presence of

#### AAV-PHP.eB-SYNpr-mitoTALEN increased $tRNA^{Ala}$ levels in the CNS of heteroplasmic $tRNA^{Ala}$ -injected mice

The main molecular phenotype of the heteroplasmic m.5024C>T mice is a decrease in  $tRNA^{Ala}$  levels due to the unstable secondary structure of the mutant  $tRNA^{Ala}$ . Therefore, we asked whether the treatment improved this molecular phenotype. Mitochondrial  $tRNA^{Ala}$  levels, determined by RT-dPCR were normalized to  $tRNA^{Asn}$  (a neighboring  $tRNA$  gene in the mtDNA that is not affected in these heteroplasmic mice). We analyzed a large series

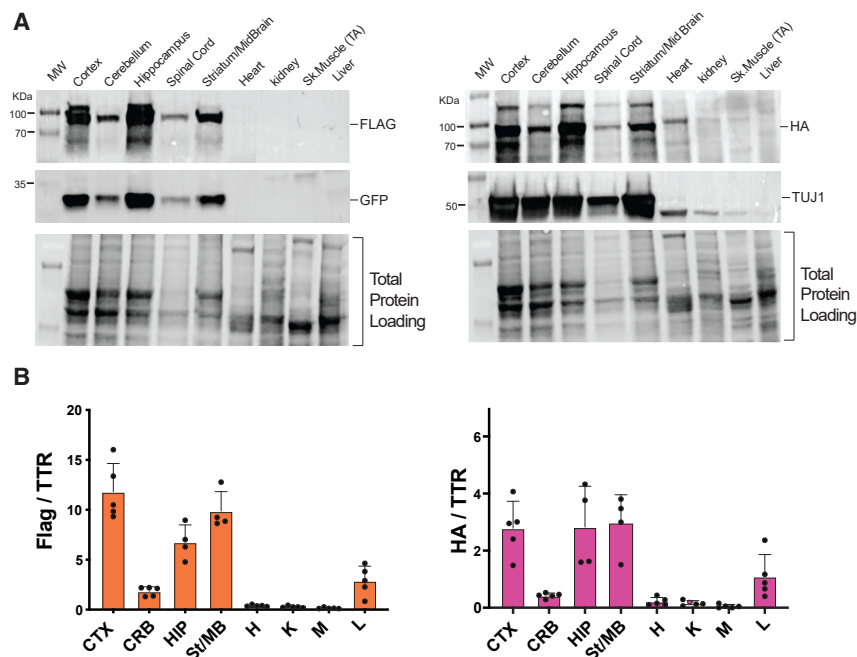


**Figure 3. CNS expression of AAV-PHP.eB-SYNpr-mitoTALEN in injected mice**

(A) P16–18 mice were retro-orbitally injected with AAV-PHP.eB-SYNpr-mitoTALEN and tissues analyzed by western blots for Flag and HA (tags present in each monomer). Neuron-specific TuJ1 was also analyzed in CNS homogenates. Predicted size of the monomers were: #1 = 100.9 kDa, #2 = 90.0 kDa and eGFP = 27.2 kDa. (B) AAV DNA quantification with primer/probes specific for Flag or HA normalized to a nuclear gene (TTR) showing high viral levels in the CNS tissues with high mitoTALEN expression. CRB, cerebellum; CTX, brain cortex; H, heart; K, kidney; L, liver; HIP, hippocampus; M, TA skeletal muscle; St/MB, striatum/midbrain. Error Bars=+SD.

insertions and deletions (INDELS) in postmortem brains by investigating homologous loci in the nuclear genome. Using the TALEN binding sequence, we performed a BLAST search and identified four homologous regions in chromosomes 2, 5, 7, and 9. These loci were amplified with primers that were specific for the nuclear loci and would not amplify the mtDNA or the other homologous loci. RFLP confirmed the nuclear origin of the amplicons (Figure S6). These fragments were subjected to next-generation sequencing (NGS) and analyzed for the presence of INDELS and SNVs. As shown in Table S3, no INDELS or SNVs were identified in the spacer between the two TALEN binding sites, which is the region undergoing a DSB. The few identified INDELS were in distant homopolymeric regions and likely the result of PCR amplification errors (Table S3).

Because BLAST may not select the closest matches for TALENs,<sup>23</sup> we also used a TALEN specific tool to nominate additional predicted off-target sites. TALENoffer is a tool for genome-wide prediction of TAL effector nuclease (TALEN) off-target sites.<sup>24</sup> We run TALENoffer taking into consideration the flexible recognition of NN RVD (for G and A). The list of nominated off-targets in descending order of specificity is shown in Table S4. We selected the top three hits for additional screenings for off-target effects in the nucleus (loci in chromosomes 15, 12, and 5). The Chr 15 (a gap of 20 bp) and Chr 5 (a gap of 13 bp) loci had higher chances of being a target than the WT mtDNA sequence (third in the TALENoffer ranking list), reflecting the importance of T0 present in the mutant mtDNA target. NGS analysis of these regions showed no Indels and no differences between the AAV-PHP.eB-GFP and AAV-PHP.eB-SYNpr-mitoTALEN.

## DISCUSSION

Although a global reduction of mutant mtDNA would be desirable for the treatment of mitochondrial diseases, it is important to understand how individual cell types behave during these treatments. Because of the prevalence of neuropathy in patients with mitochondrial diseases,<sup>25,26</sup> we specifically targeted neurons to study whether they can be treated with mitoTALEN. Although success has been achieved targeting mitochondrial mutations both *in vitro*<sup>27–30</sup> and in muscle/heart<sup>14,31,32</sup> using gene editing tools, such as mitoTALEN, mitoZFN, or mitoMeganucleases, no studies have treated the CNS. However, neurologic manifestations are among the most severe consequences of mitochondrial diseases.<sup>33,34</sup> Approximately 20% of the basal oxygen of the body is consumed by the brain for different functions. Compared with other tissues, the brain contains the highest concentration of mitochondria, since it uses much more oxygen, glucose, and energy.<sup>35</sup> The proper regulated mitochondrial dynamics; trafficking between soma, axon, and presynaptic boutons; ATP synthesis; Ca<sup>2+</sup> signaling; ROS generation; and other mitochondria-mediated intracellular signaling are essential to maintain brain homeostasis.<sup>36,37</sup> Neurons rely on mitochondrial energy production for survival, making them susceptible to mitochondria-mediated bioenergetic defects.<sup>38</sup> Moreover, neurons have specific features, such as long processes containing mitochondria, that could affect how they respond to gene editing. Our results showed that neurons are amenable to mutant mtDNA reduction by mitoNucleases. Although we obtained changes in heteroplasmy of relatively smaller amplitudes (15%–20%), this amplitude was enough to repair the molecular defect (in this case, decreased mitochondrial tRNA<sup>Ala</sup> levels).

It is not surprising that the reductions in mutant mtDNA load were relatively modest (approximately 20%) when measured in homogenates, as glial cells would not have their mtDNA mutant levels altered by the SYN promoter-driven expression of mitoTALEN. However, even small changes in heteroplasmy can have major beneficial consequences to neurons, as these could cross the threshold levels for phenotypical manifestations. We have shown that by improving mitochondrial tRNA<sup>Ala</sup> levels after a decrease in mutant

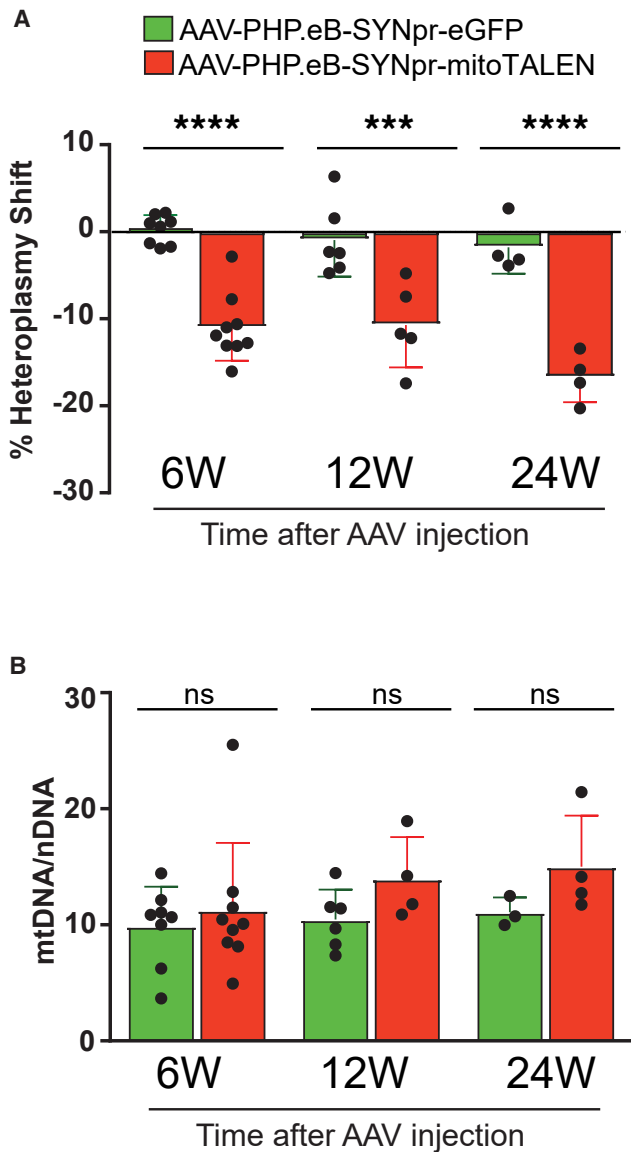


**Figure 4. Mutant mtDNA reduction in the CNS without total mtDNA copy number alterations in AAV-PHP.eB-SYNpr-mitoTALEN injected mice**

(A) DNA samples from cortex and TA from tRNA<sup>Ala</sup> mice injected at P16–18 with AAV-PHP.eB-SYNpr-mitoTALEN and PHP.eB-SYNpr-eGFP were extracted at 6, 12, and 24 weeks after systemic injection. DNA analysis by dPCR showed a significant decrease in the mutant mtDNA (m.5024C>T mutation) in cortex (transduced tissue) normalized to TA (not transduced tissue) when compared with mice injected with AAV-PHP.eB-SYNpr-eGFP. (B) No difference in the mtDNA copy number was observed in the cortex (CNS tissues expressing the mitoTALEN\*\*\*p < 0.005; \*\*\*\*p < 0.0001; ns, not significant. Unpaired t test. Error Bars=+SD.

mtDNA load by approximately 20%. In fact, the correlation between m.5024T mutation load and the tRNA alanine levels was very strong in both muscle and brain ( $R > 0.96$ ). In agreement to the slope observed in the brain analysis, the mitoTALEN treatment changed both mutation load and tRNA alanine levels by approximately the

same magnitude (–20% for mutant mtDNA and +20% for tRNA alanine levels). mtDNA copy number regulation is another key feature to be monitored when delivering mitoNucleases to the mitochondria. Decreased mtDNA copy number has been previously described in cultured cells when mutant mtDNA levels are high.<sup>29</sup> We did not detect any decrease in total mtDNA copy number in the CNS of mice injected with AAV-PHP.eB-SYNpr-mitoTALEN, at any of the time-points analyzed. We observed similar results when targeting skeletal muscle and heart with mitoTALEN,<sup>14</sup> confirming its specificity. Although we have not observed a decrease in mtDNA levels, different dosages and modifications of regulatory elements in the therapeutic gene construct could be used if this becomes a concern.

Injected mice showed no overt phenotypic alterations. Moreover, the strict mitochondrial localization and the requirement of mitoTALEN obligatory heterodimeric architecture for cleavage provide additional levels of safety. Because mtDNA pseudogenes have been found in the nuclear genome, we also searched for nuclear off-target DSBs in seven nuclear loci with high homology to the TALEN binding domain. NGS analysis of amplicons from these loci from all brain samples showed no differences in INDELS or SNVs in the mitoTALEN-treated vs. GFP-treated controls, supporting the specificity of the approach. Before entering the clinics, a more extensive and deeper search for off-targets may be required, but it is important to emphasize that most, if not all, mitoTALEN localizes to the mitochondria, decreasing the risk of nuclear off-target.

Currently, at least 14 types of CNS diseases have been experimentally treated using AAV vectors. Different ways of delivery have been used to target the CNS, including intraparenchymal, intra-CSF (intra-thecal, intra-cisterna magna, and intra-cerebroventricular), and intravenous delivery, the latter being the less invasive. Recombinant AAV vectors (rAAV) have packaging size limited to approximately 4.7 kb, which is a drawback when cloning large inserts such as TALEN monomers.<sup>39</sup> This limited capacity can be circumvented by monomeric mitoNucleases.<sup>32,40,41</sup> However, mitoTALEN still offers a high degree of specificity and ease of design.<sup>42–44</sup> Moreover, AAV allows for multiplicity of infection, making the delivery of a dimeric molecular therapy effective.

Naturally occurring AAV serotypes tend to target non-CNS tissues, specially the liver, with limited transduction efficiency in the brain due mostly to the blood-brain barrier.<sup>45</sup> In the last few years, capsid modifications,<sup>46</sup> inclusion of cell-type-specific promoters,<sup>47</sup> and enhancers<sup>48</sup> have improved specificity and expression in non-liver tissues. Viral capsids were engineered to alter their tissue tropism, such as the variants AAV-PHP.B and AAV-PHP.eB, which cross the blood-brain barrier after intravenous administration, broadly transducing CNS neurons.<sup>19,20</sup> However, this enhanced CNS tropism is restricted to the model in which these variants were selected, i.e., the C57BL/6 mouse strain. AAV-PHP.eB is unable to transduce neurons in non-human primates or other mouse strain such as BALB/c with the same efficiency.<sup>49</sup>

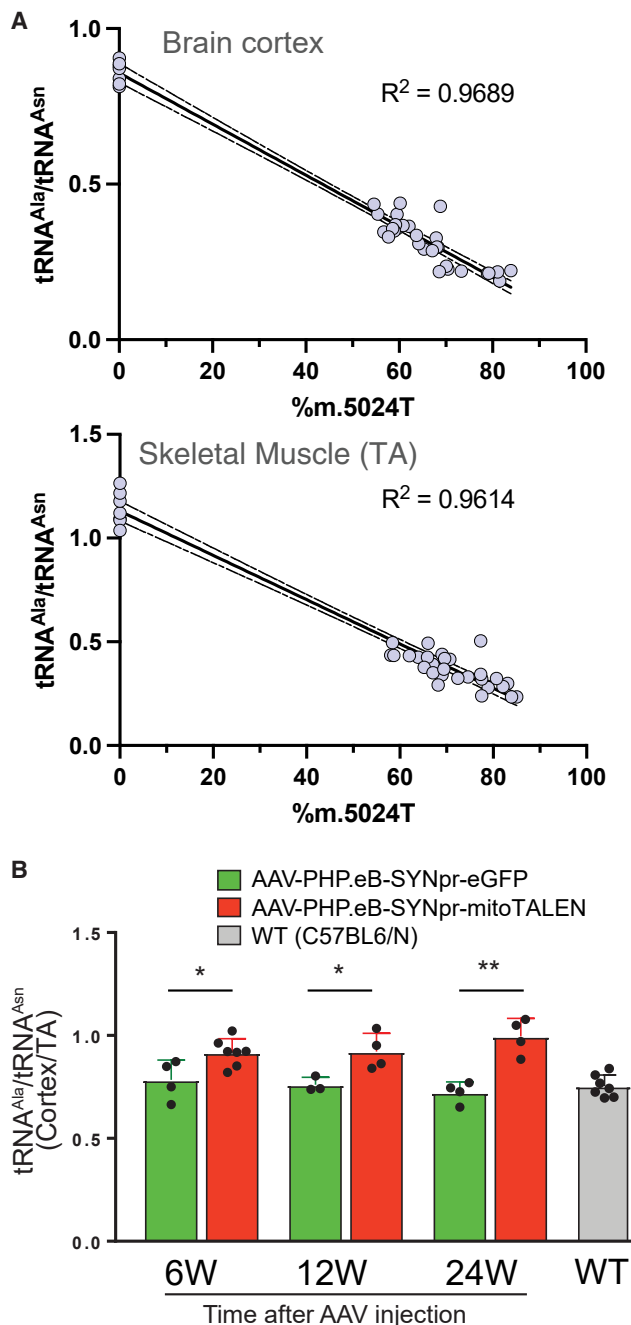


**Figure 5.  $tRNA^{Ala}$  levels were increased in the AAV-PHP.eB-SYNpr-mitoTALEN-injected mice**

(A) A tight inverse correlation between  $tRNA^{Ala}/tRNA^{Asn}$  ratios and the m.5024C>T levels was observed in brain tissue (cortex) and skeletal muscle (TA muscle) of heteroplasmic mice. Dashed lines show the 95% confidence interval. (B) Heteroplasmic mice injected with AAV-PHP.eB-SYNpr-mitoTALEN showed a significant recovery of  $tRNA^{Ala}$  levels at 6, 12, and 24 weeks. The brain heteroplasmy data were normalized to muscle as a control for heteroplasmy differences between mice. These differential ratios were not observed in the mice injected with AAV-PHP.eB-SYNpr-eGFP or in the WT, C57/BL6N mice. \* $p < 0.05$ ; \*\* $p < 0.005$ . Unpaired t test. Error Bars = +SD.

Long-term immunological reactions are additional challenges for rAAV-based gene therapies because of the continuous presence of viral particles.<sup>50</sup> The possible immunogenicity that might be developed toward the vector is another limitation to AAV gene therapies in general. This immunogenicity prevents repeated dosing, which might be necessary to ensure optimal levels of transgene expression in gene therapy of mendelian genes.<sup>51</sup> However, this would be less of a problem for mtDNA heteroplasmy reduction, as a single wave of expression should decrease the mutant mtDNA load below a threshold for phenotypic expression.

Despite the recent excitement from the discovery and use of mtDNA base editors, we still see some advantages in using mitoNucleases for most pathogenic mtDNA mutations. In fact, these two technologies could also be combined in the future, as shown in fertilized mouse oocytes.<sup>52</sup> Specific base editing of mtDNA in the heart of neonatal and adult mice has been described, showing its potential translation to human somatic gene correction therapies.<sup>53–55</sup> However, its sequence requirements restrict them to a few pathogenic mtDNA mutations and to date have been used mostly to create disease models.<sup>56,57</sup> Another deaminase, termed TALE-linked deaminases induce targeted A-to-G editing in human cells,<sup>58</sup> but more data are needed to establish its usefulness. Moreover, the applicability of mitoBase editors is also limited to possible off-target editing in the mtDNA target site.<sup>59</sup>

In this study, we showed, for the first time, that mitoTALEN can effectively target mutant mtDNA in neurons. This platform represents an important breakthrough in the mitochondrial genome-editing field, which, we predict, will soon move toward clinical trials.

## MATERIALS AND METHODS

### Constructs and plasmids

The pAAV-CBh-mkate2-IRES-MCS plasmid, was obtained from Adgene (cat#105921). We modified it by changing the mKate2 for an eGFP sequence, using a double stranded DNA fragment (Integrated DNA Technologies, Inc [IDT]) and In-Fusion Snap Assembly Master Mix (Clontech/Takara Bio USA). We also obtained the pAAV-hSYN-eGFP (cat#50465) from Adgene.

Using the AAV2/9hSYN-eGFP-WPRE-hGH plasmid as a backbone, we constructed both mitoTALEN monomers using gBlocks (IDT) and the In-Fusion HD cloning system (cat#639636-Clontech/Takara Bio USA). The final constructs containing COX8A/Su9, an immune-tag at the N-terminus of the mature protein (HA or FLAG), and a picornaviral 2A-like sequence (T2A)<sup>60</sup> between the mitoTALEN, and the fluorescent marker for expression (eGFP) in one monomer. Obligate heterodimeric *FokI* domains<sup>43</sup> were used in the respective monomers. The TALE-132 (sense strand) has 9.5 RVDs and binds to the mutation sequence (m.5024C>T)<sup>14</sup>; the TALE-134 (anti-sense strand) binding to the WT sequence was modified from the previous report<sup>14</sup> to have 11.5 RVDs. A diagram of the binding site is shown in Figure 2A. We used an N+138/C+40 termini TALEN architecture.<sup>27,61</sup>

### Animal model

The tRNA<sup>Ala</sup> m.5024C>T mouse model was described by Kauppila et al.<sup>62</sup> We also used WT mouse (C57BL/6N) males to breed with the tRNA<sup>Ala</sup> heteroplasmic females. All procedures with mice were approved by the University of Miami Miller School of Medicine IACUC.

### Virus preparation and administration

Recombinant AAV2/PHP.eB particles were produced at the University of Iowa, Viral Core Facility. The following titers were obtained:

AAV2/PHP.eB-CBh-eGFP-WPRE-SV40pA =  $6.9e^{12}$  vg/mL

AAV2/PHP.eB-hSYN-eGFP-WPRE-hGH =  $1.2e^{13}$  vg/mL

AAV2/PHP.eB-hSYN-C8S9-HA-FokI NEL-eGFP-9.5RVD =  $5.2e^{12}$  vg/mL

AAV2/PHP.eB-hSYN-C8S9-Flag-FokI CKK-11.5RVD =  $3.9e^{13}$  vg/mL

Toe DNA of heteroplasmic tRNA<sup>Ala</sup> mice were obtained at P5, before performing the injections to determine basal levels of heteroplasmy. For systemic delivery, mice at P16/18 were subjected to retro-orbital injection with 2.0–4.0e<sup>13</sup> vg/kg in a 40- $\mu$ L final volume in saline. When injecting mitoTALEN, both monomers were delivered together (total 4e<sup>13</sup> vg/kg). All injections were carried out using a short insulin syringe with a 31G needle (Becton Dickinson). Tail tissue was obtained before injection. At 6, 12, and 24 weeks after injection, mice were deeply anesthetized and perfused with chilled PBS, and skeletal, cardiac tissues, liver, kidney samples and different areas of the brain (cortex, cerebellum, hippocampus, striatum/midbrain, and spinal cord) were obtained.

### Mitochondrial expression of the mitoTALENs

For western blot studies, 40  $\mu$ g total proteins from cellular and tissue homogenates were subjected to electrophoresis in 10% mini-protein stain-free gels (BioRad cat#4568034) and transferred to polyvinylidene difluoride membranes using the Trans Blot Turbo system (BioRad cat#170-4155) according to the manufacturer's instructions. Membranes were developed with SuperSignal West Pico chemiluminescent substrate (34080, Thermo Fisher Scientific). The use of TGX Stain-Free Precast Gels allowed the determination of protein loading through gel activation with the imager. Western blots were detected by BioRad Chemidoc Image Lab Version 5.2.1. The following antibodies were used for western blots: rat monoclonal antibody to HA (cat#1867423; Roche Biochemical, 1:1,000), mouse monoclonal antibody to FLAG (cat#F3165; Sigma-Life Sciences, 1:1,000), rabbit polyclonal antibody against GFP (cat# SAB4301138, Sigma-Aldrich, 1; 1,000), monoclonal antibody against Tuj1/beta III tubulin-neuronal marker (cat# ab18660abcam; 1:1,000). Secondary antibodies were IgG, horseradish peroxidase (HRP)-linked antibodies rat-HRP (cat#A-5795, Sigma-Aldrich, 1:2,000), mouse-HRP (cat#7076, Cell Signaling, 1:2,000), and rabbit-HRP (cat#7074, cell Signaling, 1:2,000).<sup>27</sup>

For immunocytochemical studies, Cos7 cells were transfected with mitoTALEN plasmids for 24 h, incubated for 30 min at 37°C with 200 nmol MitoTracker Red CMXRos (cat#M7512, Invitrogen) and fixed with 2% paraformaldehyde for 20 min. Primary antibodies to HA (1:200) or FLAG (1:200) in 2% BSA in PBS were incubated overnight at 4°C. The following day, coverslips were incubated for 2 h at room temperature with secondary antibodies: Alexa Fluor 488-conjugated goat antibody to rat IgG (cat#A-11006, Invitrogen, 1:200) or goat antibody to mouse IgG (cat#A-11001, Invitrogen, 1:200) as described.<sup>63</sup>

### Immunocytochemistry experiments

After delivery of the virus, mice were anesthetized and perfused with chilled PBS. For histological studies, half brain was infused in cold paraformaldehyde 4% in PBS for 1 h and then sucrose 30% in PBS ON, frozen in liquid-nitrogen-cooled isopentane solution and stored at –80°C. Sections were obtained using a cryostat (18  $\mu$ m) and slides were mounted with Dapi-mounting media (Biotium cat#23004).<sup>63</sup> Images were recorded using EVOS FL Cell Imaging System (Thermo Fisher Scientific).

### Quantification of m.5024C>T mutation load, mtDNA copy number, and DNA viral titer

Total genomic DNA from different tissue after dissection was extracted with phenol-chloroform method.<sup>63</sup>

### RFLP-“last-cycle hot” PCR

PCR amplicons were obtained using the following set of primers:

Forward: 5'-CCTAGCTATCATAAGCACAA-3'

Backward: 5'-AAGCAATTGATTTGCATTCAATAGATGTAGGATGAAGTCCTGCA-3'

Amplicons were generated in a reaction containing 1 $\times$  DreamTaq green buffer (Thermo Fisher Scientific), 75 nmol of each primer, 5  $\mu$ mol of dNTPs, and 1 U DreamTaq polymerase (Thermo Fisher Scientific) in a final volume of 20  $\mu$ L. Cycling conditions were as follows: 1 cycle of 94°C for 3 min, 30 cycles of 94°C for 30 s, 59°C for 30 s, 72°C for 45 s, one cycle of 72°C for 4 min, and 12°C hold. Resulting PCR products (174 bp) were subjected to one additional cycle with dCTP, [ $\alpha$ -<sup>32</sup>P] (Perkin Elmer-cat #NEG013H100UC),<sup>64</sup> which visualizes only nascent amplicons and removes interference from hetero-duplexes formed during melting and annealing cycles. Upon PCR amplification, the WT allele for the m.5024C>T mutation, together with a 1-bp mismatched oligonucleotide primer, creates a restriction site for *Pst*I not present in the PCR product originated from the mutant mtDNA. Labeled products were digested with 0.5  $\mu$ L *Pst*I (NEB, 20U/ $\mu$ L). *Pst*I generates 2 fragments (136 and 40 bp) and resolved in a 12% polyacrylamide gel. The radioactive signal was quantified using a Cyclone phosphor-imaging system (PerkinElmer) and OptiQuant software Version 5.0.<sup>14</sup>

### **dPCR for heteroplasmy and copy number**

We use The QIAcuity dPCR System (QIAcuityOne, 5plex device-ID: 911021) to quantify mtDNA heteroplasmy and copy number. We multiplex using three sets of primer/probes as described below.<sup>65</sup> The tRNA<sup>Ala</sup>-WT probe produces two positive partitions populations that could be separated based on differences in fluorescence amplitude. These different populations were used to calculate the percentage of mutant mtDNA.<sup>65</sup> For copy number analyses, we use the ratio of mtND5 (as a mtDNA reference) and the 18S rRNA (as a nuclear reference). dPCR was performed in 24 well/nanoplates 8.5K (QIAGEN) with 12  $\mu$ L total reaction volume containing 4 $\times$  QIAcuity probe master mix (QIAGEN), 0.4  $\mu$ M of each probe, 1.6  $\mu$ M of each primer, 0.25 U/ $\mu$ L EcoRI-HF, and 0.2 ng genomic DNA. Cycling conditions were as follows: 1 cycle of 95°C for 2 min, 40 cycles of 95°C for 15 s, and 57°C for 1 min. Results were analyzed with the QIAcuity Software Suite (QIAGEN), the thresholds were manually placed on the 1D plots, and the final dPCR output was processed on Excel365.

### **Primers and probes**

#### **Mus-tRNA<sup>Ala</sup> WT (BioSearch)**

Forward primer: 5'-GCCTTCAAAGCCCTAAGA-3'

Reverse primer: 5'-CGGCGGTAGAAGTAGATTG-3'

Probe: 5'-/FAM/AACTTCTGATAAGGACTGTAAGAC/BHQplus/- 3'

Assay length: 195 bp.

#### **MT-ND5 (IDT)**

Forward primer: 5'-CCTGAGCCCTACTAATTACAC

Reverse primer: 5'-GAGATGACAAATCCTGCAAAG

Probe: 5'/HEX/ACCCAATCAAACGCCTAGCATTTCG/- 3'

Assay length = 190 bp.

#### **Mus-18S rRNA-NUCLEAR (IDT)**

Forward primer: 5'-CGTCTGCCCTATCAACTTT-3'

Reverse primer: 5'-CCTCGAAAGAGTCCTGTATTG-3'

Probe: 5'-/5Cy5/AGAAACGGCTACCACATCC/3IAbRQSp/- 3'

Assay length = 114 bp.

### **AAV DNA quantification**

Genomic DNA from cortex and TA muscle of injected mice with AAV-PHP.eB-SYNpr-mitoTALEN was extracted as described previously. dPCR was performed using a set of primers and probes to target the tags present in the construct, Flag, and HA and normalized to the nuclear gene TTR. dPCR was performed as described above.

### **Primers and probes**

#### **Mus-AAV-HA (IDT)**

Forward primer: 5'-TTACGATGTGCTGACTACG-3'

Reverse primer: 5'-TCTGGCACGTCATAGGG-3'

Probe: 5'-/FAM/AATCGGGCA/ZEN/CGTCGTATGGATAGC/3IAbkFQ/- 3'

Assay length = 75 bp.

#### **Mus-AAV-Flag (IDT)**

Forward primer: 5'-AAGGATCACGACGGCGATTA-3'

Reverse primer: 5'-ATCGGTGCCCTTGTCTG-3'

Probe: 5'-/TAMN/AGGACCACGATATCGACTACAAAGACGA/3IAbRQSp/- 3'

Assay length: 69 bp.

#### **Mus-TTR (IDT)**

Forward primer: 5'-GACAGGATGGCTTCCCTTC-3'

Reverse primer: 5'-GTCTAACTGCCATGTCTGGAT-3'

Probe: 5'-/Cy5/CCTCGCTGG/TAO/ACTGGTATTTGTGTCT/3IAbRQSp/- 3'

### **RNA isolation from mouse samples**

RNA from 10–40  $\mu$ g tissue was extracted using the TRIZOL reagent (Invitrogen, cat #15596026) as per manufacturer's instructions. Muscle samples were snap frozen in liquid N<sub>2</sub> and pulverized with a mortar. The pulverized tissue was resuspended in TRIZOL reagent and homogenized using a VWR Pellet Mixer (VWR, cat #431-0100) and disposable pestles (Argos Technologies Inc., cat #7339-901). Brain tissue was instead directly homogenized in TRIZOL reagent and processed as suggested by the manufacturer.

### **tRNA retro-transcription and quantification by dPCR**

Purified total RNA extracted from tissue was used as the starting material for a retro-transcription using the MultiScribe Reverse Transcriptase (Invitrogen, cat #4311235) in aseptic conditions and employing materials either certified RNase-free or washed with RNaseZap RNase Decontamination Solution (Invitrogen, cat #AM9780). In short, 10 ng total RNA template was mixed with 1  $\mu$ M the forward primer (LNA-modified [+]) for mt-tRNA<sup>Ala</sup> (TGTAAGA+GA+CTTCATCCTAC) and mt-tRNA<sup>Asn</sup> (GAATTTAAA+C+CTACGAAA) in the presence of the transcriptase (50 U/r.) and RNase Inhibitor (Applied Biosystems, cat#N8080119, 4 U/r.). Then, the reaction was incubated in the following thermoblock program: (1) 16°C, 30 min; (2) 42°C, 30 min; (3) 85°C, 5 min; and (4) keep at 4°C till use. Controls with no RT were also run in parallel for each sample.

The unpurified reaction was then used as the cDNA template for the dPCR to quantify the tRNA<sup>Ala</sup> and tRNA<sup>Asn</sup> following the manufacturer's instructions. A ratio tRNA<sup>Ala</sup> to tRNA<sup>Asn</sup> was calculated. Briefly, the unpurified cDNA was first diluted in RNase-free mQ-H<sub>2</sub>O (1/100 dilutions for brain samples, 1/200 dilutions for muscle samples) and then the dPCR reaction was run on a QIAcuity One, 5plex Device (Qiagen, # 911021) on 24-well, 8.5k Nanoplates (Qiagen, #250011). In short, each dPCR final reaction consisted of 1× of QIAcuity Probe PCR Kit Master Mix, (Qiagen, #250103), 0.5 μM of the corresponding forward and reverse primers for mt-tRNA<sup>Ala</sup> and mt-tRNA<sup>Asn</sup>, and 0.25 μM of their corresponding probe. The dPCR plate was loaded in parallel with both the transcriptase reactions and no transcriptase controls, and cycling conditions were as follows: on cycle 95°C for 2 min; 40 cycles: 95°C for 15 s; and 50°C for 1 min; and results were analyzed as described previously. Primers and probes were modified to contain LNA [+] or MGB additions, which increases the TM.

#### **Mus-mt-tRNA<sup>Ala</sup> (IDT)**

Forward primer: 5'-TGTAAGA+CTTCATCCTAC-3'

Reverse primer: 5'-TTAGCTTAATTAAGCAATTG-3'

Probe: 5'-/FAM/CTATTGAATGCAAATCAA/MGB-3' (Applied Biosystems)

Assay length: 56 bp.

#### **Mus-mt-tRNA<sup>Asn</sup> (IDT)**

Forward primer: 5'-GAATTTAAA+C+CTACGAAA-3'

Reverse primer: 5'-GATTGAA+GC+CAGTAATA-3'

Probe: 5'-/HEX/TTTA+GTTAA+CA+G+CTAAATAC-3'

Assay length: 57 bp.

#### **Analysis of NUMTS pseudogenes as potential contributors to mtDNA heteroplasmy levels**

We amplified total DNA with primer sets common to mtDNA and to two nuclear NUMTS pseudogenes (chr2 and 5). As a control, we used total DNA from a mouse rho zero cell line. The resulting amplicons were analyzed by Sanger sequence.

#### **Primers**

MtCh5Ch2-F1 CCAACCTAATATTTTCCACCCT

MtCh5Ch2-B1 GGCGGTAGAAGTAGATTGAA

#### **Nominated nuclear off-target of mitoTALEN identified by BLAST**

We amplified NUMTS pseudogenes with specific primers (listed below). Amplicons were tested by RFLP (*Xba*I for Ch.2, 5 and 7; *Bsp*QI for Ch9) to ensure they were not originated from mtDNA. Amplicons were then subjected to NGS (Azenta Life Sciences, Amplicon-

EZ). INDELS and SNVs were analyzed by splitting each chromosome into a separate fasta file. From this, each chromosome reference sequence was indexed by bwa v0.7.17, a faidx was created by samtools v1.13, and a sequence dictionary was created using PicardTools v2.2.1. Sample fastq files were demuxed using the first eight nucleotides of the read1 and read2 separately with an exact match to the sample barcode. Read 1 and read 2 were merged into a single long read by using fastq-join function in ea-utils (v.10c2192). Resulting fastq files after merging were aligned with bwa mem against the chromosomal reference index. Individual coverage positions were calculated using GATK's (v4.3.0.0) CollectAllelicCounts function which resulted in number of reference alleles vs. alternative alleles with the highest alternative base change. Indels were counted using the aligned bam file by extracting the CIGAR string and requiring reads to be aligned all at the same anchor position. From this a unique set of sequences with counts was calculated using standard unix tools.

#### **Primer for BLAST/NUMTS off-target analyses**

Chr2 OffTarget-F1 AGGCTCCGAATAGCAGATAT

Chr2 OffTarget-B1 CACCACTAACAGGATTTC

Chr5 OffTarget-F1 AGGGAAGAAGACTCAGAAAC

Chr5 OffTarget-B1 AGGTTAGTATTCTTAGGGGA

Chr7 OffTarget-F1 AATTCATCCCAGAGCCTTTA

Chr7 OffTarget-B1 AAAATGTCCGAGTAAGCACC

Chr9 OffTarget-F1 TTAGAAATGAATGGGGGTTG

Chr9 OffTarget-B1 AGCAATGAGTACCTAACCAA

#### **Nominated nuclear off-target of mitoTALEN identified by TALENoffer**

We ran the TALENoffer<sup>24</sup> as described. This method has been shown to successfully predict known off-targets of engineered TALENs. We used the default mode (TALgetter model) that does not infer strict specificities (e.g., allowing for non-T at position zero, and allows for A or G for NN RVD). TALgetter is the recommended model for most TALEN searches.

#### **Primer for TALENoffer/NUMTS off-target analyses**

Chr15 OffTarget-F1 CTAAGTGCAGAGAATGACAT

Chr15 OffTarget-B1 CTCTTGGCTGTGTTCTTGTTA

Chr5n OffTarget-F1 TAACTTTATCCTTCCTTCCC

Chr5n OffTarget-B1 ACAGGTGTAAAGGACTAACT

Chr12 OffTarget-F1 TAATGTGTCTGTGGGCTTCA

Chr12 OffTarget-B1 GAGTAAAAGCCTAAAGATGG

### Statistical analyses

All data analysis was performed using GraphPad Prism 7 and 8. All statistics are presented as mean  $\pm$  SEM. Pairwise comparisons were performed using the unpaired two-tailed Student t test, and p values of 0.05 or less were considered significant.

### DATA AND CODE AVAILABILITY

Data that are not already included in the manuscript is available upon request.

### SUPPLEMENTAL INFORMATION

Supplemental information can be found online at <https://doi.org/10.1016/j.omtn.2024.102132>.

### ACKNOWLEDGMENTS

This work was funded primarily by the National Institutes of Health (NIH) Grant 5R01EY010804 with secondary support from 1R01NS079965, the Florida Department of Health (21K05), the Muscular Dystrophy Association (MDA 964119), and the Army Research Office (W911NF-21-1-0248). J.B.S. is supported by MRC award MC\_PC\_21046 to establish an MRC National Mouse Genetics Network Mitochondria Cluster (MitoCluster).

### AUTHOR CONTRIBUTIONS

S.B. and C.T.M. designed the experiments and wrote the paper; S.B., J.D.B.-P., and M.P. conducted experiments; J.B.S. produced the heteroplasmic mouse; D.V.B. and A.J.G. performed the NGS analysis. All authors contributed to the editing the manuscript.

### DECLARATION OF INTERESTS

J.B.S. is a named inventor for corporate licensing agreements offered by Max Planck Innovation, for commercial use of the mt-TA C5024T mice. The other authors declare no competing interests.

### REFERENCES

- Nunnari, J., and Suomalainen, A. (2012). Mitochondria: in sickness and in health. *Cell* 148, 1145–1159. <https://doi.org/10.1016/j.cell.2012.02.035>.
- Spinelli, J.B., and Haigis, M.C. (2018). The multifaceted contributions of mitochondria to cellular metabolism. *Nat. Cell Biol.* 20, 745–754. <https://doi.org/10.1038/s41556-018-0124-1>.
- Taanman, J.W. (1999). The mitochondrial genome: structure, transcription, translation and replication. *BBA* 1410, 103–123.
- Gustafsson, C.M., Falkenberg, M., and Larsson, N.G. (2016). Maintenance and Expression of Mammalian Mitochondrial DNA. *Annu. Rev. Biochem.* 85, 133–160. <https://doi.org/10.1146/annurev-biochem-060815-014402>.
- Gorman, G.S., Schaefer, A.M., Ng, Y., Gomez, N., Blakely, E.L., Alston, C.L., Feeny, C., Horvath, R., Yu-Wai-Man, P., Chinnery, P.F., et al. (2015). Prevalence of nuclear and mitochondrial DNA mutations related to adult mitochondrial disease. *Ann. Neurol.* 77, 753–759. <https://doi.org/10.1002/ana.24362>.
- Schon, E.A., DiMauro, S., and Hirano, M. (2012). Human mitochondrial DNA: roles of inherited and somatic mutations. *Nat. Rev. Genet.* 13, 878–890. <https://doi.org/10.1038/nrg3275>.
- Schaefer, A.M., McFarland, R., Blakely, E.L., He, L., Whittaker, R.G., Taylor, R.W., Chinnery, P.F., and Turnbull, D.M. (2008). Prevalence of mitochondrial DNA disease in adults. *Ann. Neurol.* 63, 35–39. <https://doi.org/10.1002/ana.21217>.
- Ruiz-Pesini, E., Lott, M.T., Procaccio, V., Poole, J.C., Brandon, M.C., Mishmar, D., Yi, C., Kreuziger, J., Baldi, P., and Wallace, D.C. (2007). An enhanced MITOMAP with a global mtDNA mutational phylogeny. *Nucleic Acids Res.* 35, D823–D828. <https://doi.org/10.1093/nar/gkl927>.
- Viscomi, C., Bottani, E., and Zeviani, M. (2015). Emerging concepts in the therapy of mitochondrial disease. *Biochim. Biophys. Acta* 1847, 544–557. <https://doi.org/10.1016/j.bbabi.2015.03.001>.
- Gorman, G.S., Chinnery, P.F., DiMauro, S., Hirano, M., Koga, Y., McFarland, R., Suomalainen, A., Thorburn, D.R., Zeviani, M., and Turnbull, D.M. (2016). Mitochondrial diseases. *Nat. Rev. Dis. Primers* 2, 16080. <https://doi.org/10.1038/nrdp.2016.80>.
- Barrera-Paez, J.D., and Moraes, C.T. (2023). Mitochondrial genome engineering coming-of-age: (Trends in Genetics, 38:869-880, 2022). *Trends Genet.* 39, 89. <https://doi.org/10.1016/j.tig.2022.08.002>.
- Zekonyte, U., Bacman, S.R., and Moraes, C.T. (2020). DNA-editing enzymes as potential treatments for heteroplasmic mtDNA diseases. *J. Intern. Med.* 287, 685–697. <https://doi.org/10.1111/joim.13055>.
- Falabella, M., Minczuk, M., Hanna, M.G., Viscomi, C., and Pitceathly, R.D.S. (2022). Gene therapy for primary mitochondrial diseases: experimental advances and clinical challenges. *Nat. Rev. Neurol.* 18, 689–698. <https://doi.org/10.1038/s41582-022-00715-9>.
- Bacman, S.R., Kauppila, J.H.K., Pereira, C.V., Nissanka, N., Miranda, M., Pinto, M., Williams, S.L., Larsson, N.G., Stewart, J.B., and Moraes, C.T. (2018). MitoTALEN reduces mutant mtDNA load and restores tRNA(Ala) levels in a mouse model of heteroplasmic mtDNA mutation. *Nat. Med.* 24, 1696–1700. <https://doi.org/10.1038/s41591-018-0166-8>.
- Aldossary, A.M., Tawfik, E.A., Alomary, M.N., Alsudir, S.A., Alfahad, A.J., Alshehri, A.A., Almughem, F.A., Mohammed, R.Y., and Alzaydi, M.M. (2022). Recent advances in mitochondrial diseases: From molecular insights to therapeutic perspectives. *Saudi Pharmaceut. J.* 30, 1065–1078. <https://doi.org/10.1016/j.jsps.2022.05.011>.
- Mancuso, M. (2023). Complex neurological and multisystem presentations in mitochondrial disease. *Handb. Clin. Neurol.* 194, 117–124. <https://doi.org/10.1016/B978-0-12-821751-1.00003-8>.
- Finnilä, S., Tuisku, S., Herva, R., and Majamaa, K. (2001). A novel mitochondrial DNA mutation and a mutation in the Notch3 gene in a patient with myopathy and CADASIL. *J. Mol. Med.* 79, 641–647. <https://doi.org/10.1007/s001090100268>.
- McFarland, R., Swalwell, H., Blakely, E.L., He, L., Groen, E.J., Turnbull, D.M., Bushby, K.M., and Taylor, R.W. (2008). The m.5650G>A mitochondrial tRNAAla mutation is pathogenic and causes a phenotype of pure myopathy. *Neuromuscul. Disord.* 18, 63–67. <https://doi.org/10.1016/j.nmd.2007.07.007>.
- Chan, K.Y., Jang, M.J., Yoo, B.B., Greenbaum, A., Ravi, N., Wu, W.L., Sánchez-Guardado, L., Lois, C., Mazmanian, S.K., Deverman, B.E., and Gradinaru, V. (2017). Engineered AAVs for efficient noninvasive gene delivery to the central and peripheral nervous systems. *Nat. Neurosci.* 20, 1172–1179. <https://doi.org/10.1038/nn.4593>.
- Deverman, B.E., Pravdo, P.L., Simpson, B.P., Kumar, S.R., Chan, K.Y., Banerjee, A., Wu, W.L., Yang, B., Huber, N., Pasca, S.P., and Gradinaru, V. (2016). Cre-dependent selection yields AAV variants for widespread gene transfer to the adult brain. *Nat. Biotechnol.* 34, 204–209. <https://doi.org/10.1038/nbt.3440>.
- Radhiyanti, P.T., Konno, A., Matsuzaki, Y., and Hirai, H. (2021). Comparative study of neuron-specific promoters in mouse brain transduced by intravenously administered AAV-PHP.eB. *Neurosci. Lett.* 756, 135956. <https://doi.org/10.1016/j.neulet.2021.135956>.
- Tsai, S.Q., Zheng, Z., Nguyen, N.T., Liebers, M., Topkar, V.V., Thapar, V., Wyvekens, N., Khayter, C., Iafrate, A.J., Le, L.P., et al. (2015). GUIDE-seq enables genome-wide profiling of off-target cleavage by CRISPR-Cas nucleases. *Nat. Biotechnol.* 33, 187–197. <https://doi.org/10.1038/nbt.3117>.
- Bao, X.R., Pan, Y., Lee, C.M., Davis, T.H., and Bao, G. (2021). Tools for experimental and computational analyses of off-target editing by programmable nucleases. *Nat. Protoc.* 16, 10–26. <https://doi.org/10.1038/s41596-020-00431-y>.
- Grau, J., Boch, J., and Posch, S. (2013). TALENoffer: genome-wide TALEN off-target prediction. *Bioinformatics* 29, 2931–2932. <https://doi.org/10.1093/bioinformatics/btt501>.

25. Beaudin, M., Manto, M., Schmahmann, J.D., Pandolfo, M., and Dupre, N. (2022). Recessive cerebellar and afferent ataxias - clinical challenges and future directions. *Nat. Rev. Neurol.* 18, 257–272. <https://doi.org/10.1038/s41582-022-00634-9>.
26. Horvath, R., Medina, J., Reilly, M.M., Shy, M.E., and Zuchner, S. (2023). Peripheral neuropathy in mitochondrial disease. *Handb. Clin. Neurol.* 194, 99–116. <https://doi.org/10.1016/B978-0-12-821751-1.00014-2>.
27. Bacman, S.R., Williams, S.L., Pinto, M., Peralta, S., and Moraes, C.T. (2013). Specific elimination of mutant mitochondrial genomes in patient-derived cells by mitoTALENs. *Nat. Med.* 19, 1111–1113. <https://doi.org/10.1038/nm.3261>.
28. Hashimoto, M., Bacman, S.R., Peralta, S., Falk, M.J., Chomyn, A., Chan, D.C., Williams, S.L., and Moraes, C.T. (2015). MitoTALEN: A General Approach to Reduce Mutant mtDNA Loads and Restore Oxidative Phosphorylation Function in Mitochondrial Diseases. *Mol. Ther.* 23, 1592–1599. <https://doi.org/10.1038/mt.2015.126>.
29. Gammage, P.A., and Minczuk, M. (2018). Enhanced Manipulation of Human Mitochondrial DNA Heteroplasmy In Vitro Using Tunable mtZFN Technology. *Methods Mol. Biol.* 1867, 43–56. [https://doi.org/10.1007/978-1-4939-8799-3\\_4](https://doi.org/10.1007/978-1-4939-8799-3_4).
30. Gammage, P.A., Gaude, E., Van Haute, L., Rebelo-Guiomar, P., Jackson, C.B., Rorbach, J., Pekalski, M.L., Robinson, A.J., Charpentier, M., Concordet, J.P., et al. (2016). Near-complete elimination of mutant mtDNA by iterative or dynamic dose-controlled treatment with mtZFNs. *Nucleic Acids Res.* 44, 7804–7816. <https://doi.org/10.1093/nar/gkw676>.
31. Gammage, P.A., Viscomi, C., Simard, M.L., Costa, A.S.H., Gaude, E., Powell, C.A., Van Haute, L., McCann, B.J., Rebelo-Guiomar, P., Cerutti, R., et al. (2018). Genome editing in mitochondria corrects a pathogenic mtDNA mutation in vivo. *Nat. Med.* 24, 1691–1695. <https://doi.org/10.1038/s41591-018-0165-9>.
32. Zekonyte, U., Bacman, S.R., Smith, J., Shoop, W., Pereira, C.V., Tomberlin, G., Stewart, J., Jantz, D., and Moraes, C.T. (2021). Mitochondrial targeted meganuclease as a platform to eliminate mutant mtDNA in vivo. *Nat. Commun.* 12, 3210. <https://doi.org/10.1038/s41467-021-23561-7>.
33. Martikainen, M.H., and Chinnery, P.F. (2015). Mitochondrial disease: mimics and chameleons. *Practical Neurol.* 15, 424–435. <https://doi.org/10.1136/practneurol-2015-001191>.
34. Riquin, E., Duverger, P., Cariou, C., Barth, M., Prouteau, C., Van Bogaert, P., Bonneau, D., and Roy, A. (2020). Neuropsychological and Psychiatric Features of Children and Adolescents Affected With Mitochondrial Diseases: A Systematic Review. *Front. Psychiatr.* 11, 747. <https://doi.org/10.3389/fpsy.2020.00747>.
35. Maurya, S.K., Gupta, S., Bakshi, A., Kaur, H., Jain, A., Senapati, S., and Baghel, M.S. (2022). Targeting mitochondria in the regulation of neurodegenerative diseases: A comprehensive review. *J. Neurosci. Res.* 100, 1845–1861. <https://doi.org/10.1002/jnr.25110>.
36. Flippo, K.H., and Strack, S. (2017). Mitochondrial dynamics in neuronal injury, development and plasticity. *J. Cell Sci.* 130, 671–681. <https://doi.org/10.1242/jcs.171017>.
37. Lee, A., Hirabayashi, Y., Kwon, S.K., Lewis, T.L., Jr., and Polleux, F. (2018). Emerging roles of mitochondria in synaptic transmission and neurodegeneration. *Curr. Opin. Physiol.* 3, 82–93. <https://doi.org/10.1016/j.cophys.2018.03.009>.
38. Kann, O., and Kovács, R. (2007). Mitochondria and neuronal activity. *Am. J. Physiol. Cell Physiol.* 292, C641–C657. <https://doi.org/10.1152/ajpcell.00222.2006>.
39. Di Donfrancesco, A., Massaro, G., Di Meo, I., Tiranti, V., Bottani, E., and Brunetti, D. (2022). Gene Therapy for Mitochondrial Diseases: Current Status and Future Perspective. *Pharmaceutics* 14, 1287. <https://doi.org/10.3390/pharmaceutics14061287>.
40. Minczuk, M., Papworth, M.A., Miller, J.C., Murphy, M.P., and Klug, A. (2008). Development of a single-chain, quasi-dimeric zinc-finger nuclease for the selective degradation of mutated human mitochondrial DNA. *Nucleic Acids Res.* 36, 3926–3938. <https://doi.org/10.1093/nar/gkn313>.
41. Pereira, C.V., Bacman, S.R., Arguello, T., Zekonyte, U., Williams, S.L., Edgell, D.R., and Moraes, C.T. (2018). mitoTev-TALE: a monomeric DNA editing enzyme to reduce mutant mitochondrial DNA levels. *EMBO Mol. Med.* 10, e8084. <https://doi.org/10.15252/emmm.201708084>.
42. Miller, J.C., Tan, S., Qiao, G., Barlow, K.A., Wang, J., Xia, D.F., Meng, X., Paschon, D.E., Leung, E., Hinkley, S.J., et al. (2011). A TALE nuclease architecture for efficient genome editing. *Nat. Biotechnol.* 29, 143–148. <https://doi.org/10.1038/nbt.1755>.
43. Doyon, Y., Vo, T.D., Mendel, M.C., Greenberg, S.G., Wang, J., Xia, D.F., Miller, J.C., Urnov, F.D., Gregory, P.D., and Holmes, M.C. (2011). Enhancing zinc-finger-nuclease activity with improved obligate heterodimeric architectures. *Nat. Methods* 8, 74–79. <https://doi.org/10.1038/nmeth.1539>.
44. Zhang, F., Cong, L., Lodato, S., Kosuri, S., Church, G.M., and Arlotta, P. (2011). Efficient construction of sequence-specific TAL effectors for modulating mammalian transcription. *Nat. Biotechnol.* 29, 149–153. <https://doi.org/10.1038/nbt.1775>.
45. Deverman, B.E., Ravina, B.M., Bankiewicz, K.S., Paul, S.M., and Sah, D.W.Y. (2018). Gene therapy for neurological disorders: progress and prospects. *Nat. Rev. Drug Discov.* 17, 641–659. <https://doi.org/10.1038/nrd.2018.110>.
46. Bedbrook, C.N., Deverman, B.E., and Gradinaru, V. (2018). Viral Strategies for Targeting the Central and Peripheral Nervous Systems. *Annu. Rev. Neurosci.* 41, 323–348. <https://doi.org/10.1146/annurev-neuro-080317-062048>.
47. Nieuwenhuis, B., Haenzi, B., Hilton, S., Carnicer-Lombarte, A., Hobo, B., Verhaagen, J., and Fawcett, J.W. (2021). Optimization of adeno-associated viral vector-mediated transduction of the corticospinal tract: comparison of four promoters. *Gene Ther.* 28, 56–74. <https://doi.org/10.1038/s41434-020-0169-1>.
48. Graybuck, L.T., Daigle, T.L., Sedeño-Cortés, A.E., Walker, M., Kalmbach, B., Lenz, G.H., Morin, E., Nguyen, T.N., Garren, E., Bendrick, J.L., et al. (2021). Enhancer viruses for combinatorial cell-subclass-specific labeling. *Neuron* 109, 1449–1464.e13. <https://doi.org/10.1016/j.neuron.2021.03.011>.
49. Hordeaux, J., Wang, Q., Katz, N., Buza, E.L., Bell, P., and Wilson, J.M. (2018). The Neurotropic Properties of AAV-PHP.B Are Limited to C57BL/6J Mice. *Mol. Ther.* 26, 664–668. <https://doi.org/10.1016/j.ymthe.2018.01.018>.
50. Rivière, C., Danos, O., and Douar, A.M. (2006). Long-term expression and repeated administration of AAV type 1, 2 and 5 vectors in skeletal muscle of immunocompetent adult mice. *Gene Ther.* 13, 1300–1308. <https://doi.org/10.1038/sj.gt.3302766>.
51. Verdera, H.C., Kuranda, K., and Mingozzi, F. (2020). AAV Vector Immunogenicity in Humans: A Long Journey to Successful Gene Transfer. *Mol. Ther.* 28, 723–746. <https://doi.org/10.1016/j.ymthe.2019.12.010>.
52. Lee, S., Lee, H., Baek, G., Namgung, E., Park, J.M., Kim, S., Hong, S., and Kim, J.S. (2022). Enhanced mitochondrial DNA editing in mice using nuclear-exported TALE-linked deaminases and nucleases. *Genome Biol.* 23, 211. <https://doi.org/10.1186/s13059-022-02782-z>.
53. Mok, B.Y., de Moraes, M.H., Zeng, J., Bosch, D.E., Kotrys, A.V., Raguram, A., Hsu, F., Radey, M.C., Peterson, S.B., Mootha, V.K., et al. (2020). A bacterial cytidine deaminase toxin enables CRISPR-free mitochondrial base editing. *Nature* 583, 631–637. <https://doi.org/10.1038/s41586-020-2477-4>.
54. Willis, J.C.W., Silva-Pinheiro, P., Widdup, L., Minczuk, M., and Liu, D.R. (2022). Compact zinc finger base editors that edit mitochondrial or nuclear DNA in vitro and in vivo. *Nat. Commun.* 13, 7204. <https://doi.org/10.1038/s41467-022-34784-7>.
55. Lee, H., Lee, S., Baek, G., Kim, A., Kang, B.C., Seo, H., and Kim, J.S. (2021). Mitochondrial DNA editing in mice with DddA-TALE fusion deaminases. *Nat. Commun.* 12, 1190. <https://doi.org/10.1038/s41467-021-21464-1>.
56. Silva-Pinheiro, P., Mutti, C.D., Van Haute, L., Powell, C.A., Nash, P.A., Turner, K., and Minczuk, M. (2023). A library of base editors for the precise ablation of all protein-coding genes in the mouse mitochondrial genome. *Nat. Biomed. Eng.* 7, 692–703. <https://doi.org/10.1038/s41551-022-00968-1>.
57. Silva-Pinheiro, P., Nash, P.A., Van Haute, L., Mutti, C.D., Turner, K., and Minczuk, M. (2022). In vivo mitochondrial base editing via adeno-associated viral delivery to mouse post-mitotic tissue. *Nat. Commun.* 13, 750. <https://doi.org/10.1038/s41467-022-28358-w>.
58. Cho, S.I., Lee, S., Mok, Y.G., Lim, K., Lee, J., Lee, J.M., Chung, E., and Kim, J.S. (2022). Targeted A-to-G base editing in human mitochondrial DNA with programmable deaminases. *Cell* 185, 1764–1776.e12. <https://doi.org/10.1016/j.cell.2022.03.039>.
59. Lei, Z., Meng, H., Liu, L., Zhao, H., Rao, X., Yan, Y., Wu, H., Liu, M., He, A., and Yi, C. (2022). Mitochondrial base editor induces substantial nuclear off-target mutations. *Nature* 606, 804–811. <https://doi.org/10.1038/s41586-022-04836-5>.
60. Szymczak, A.L., Workman, C.J., Wang, Y., Vignali, K.M., Dilioglou, S., Vanin, E.F., and Vignali, D.A.A. (2004). Correction of multi-gene deficiency in vivo using a single 'self-cleaving' 2A peptide-based retroviral vector. *Nat. Biotechnol.* 22, 589–594. <https://doi.org/10.1038/nbt957>.

61. Takasu, Y., Sajwan, S., Daimon, T., Osanai-Futahashi, M., Uchino, K., Sezutsu, H., Tamura, T., and Zurovec, M. (2013). Efficient TALEN construction for Bombyx mori gene targeting. *PLoS One* 8, e73458. <https://doi.org/10.1371/journal.pone.0073458>.
62. Kauppila, J.H.K., Baines, H.L., Bratic, A., Simard, M.L., Freyer, C., Mourier, A., Stamp, C., Filograna, R., Larsson, N.G., Greaves, L.C., and Stewart, J.B. (2016). A Phenotype-Driven Approach to Generate Mouse Models with Pathogenic mtDNA Mutations Causing Mitochondrial Disease. *Cell Rep.* 16, 2980–2990. <https://doi.org/10.1016/j.celrep.2016.08.037>.
63. Bacman, S.R., Williams, S.L., Garcia, S., and Moraes, C.T. (2010). Organ-specific shifts in mtDNA heteroplasmy following systemic delivery of a mitochondria-targeted restriction endonuclease. *Gene Ther.* 17, 713–720. <https://doi.org/10.1038/gt.2010.25>.
64. Moraes, C.T., Atencio, D.P., Oca-Cossio, J., and Diaz, F. (2003). Techniques and pitfalls in the detection of pathogenic mitochondrial DNA mutations. *J. Mol. Diagn.* 5, 197–208. [https://doi.org/10.1016/S1525-1578\(10\)60474-6](https://doi.org/10.1016/S1525-1578(10)60474-6).
65. Shoop, W.K., Gorsuch, C.L., Bacman, S.R., and Moraes, C.T. (2022). Precise and simultaneous quantification of mitochondrial DNA heteroplasmy and copy number by digital PCR. *J. Biol. Chem.* 298, 102574. <https://doi.org/10.1016/j.jbc.2022.102574>.